

Superconducting readout of current-induced magnetization switching

Cite as: Appl. Phys. Lett. **127**, 262601 (2025); doi: [10.1063/5.0310692](https://doi.org/10.1063/5.0310692)

Submitted: 4 November 2025 · Accepted: 12 December 2025 ·

Published Online: 30 December 2025



View Online



Export Citation



CrossMark

Lukas Kammermeier^{a)}  and Elke Scheer 

AFFILIATIONS

Department of Physics, University of Konstanz, 78464 Konstanz, Germany

^{a)} Author to whom correspondence should be addressed: lukas.kammermeier@uni-konstanz.de

ABSTRACT

We demonstrate a superconducting readout method for detecting current-induced magnetization switching of a polycrystalline cobalt wire, based on the measurement of the critical current of an adjacent superconducting aluminum wire. The critical current I_c of this superconductor–superconductor/ferromagnet–superconductor junction is highly dependent on the magnetization state of the ferromagnet, reflected in its local stray-field distribution. This dependency allows for a detection of changes in the magnetization of the ferromagnet while no current passes through it during readout. Furthermore, we present micromagnetic simulations replicating our observations, thereby visualizing the microscopic switching behavior in polycrystalline Co.

© 2025 Author(s). All article content, except where otherwise noted, is licensed under a Creative Commons Attribution (CC BY) license (<https://creativecommons.org/licenses/by/4.0/>). <https://doi.org/10.1063/5.0310692>

Current-induced magnetization switching (CIMS) phenomena have become central to the development of spintronic devices, offering promising routes for low-power, nonvolatile magnetic memory technologies.^{1,2}

There are many processes that are actively investigated to achieve CIMS with minimal current density J . The different device architectures exploit spin transfer torque (STT),^{3,4} spin-orbit torque (SOT),⁵ voltage-controlled magnetic anisotropy,⁶ spin Hall effect,⁷ domain-wall motion,^{8,9} and Oersted fields^{10,11} to change the magnetization configuration of a ferromagnet through application of an electric current pulse.

Equally relevant to writing a logic bit with CIMS is its readout. The common way to detect magnetization switching is through tunneling magnetoresistance¹² or giant magnetoresistance^{1,13} and more recently through the anomalous Hall effect.¹⁴ All these methods require a dissipative current passing through the magnet while reading. Especially in low-temperature superconducting computing, low power dissipation is highly desirable for reducing thermal load and enabling high integration density, e.g., of superconducting memory elements.

In this study, we present a measurement technique based on a superconducting junction placed in close proximity to the ferromagnetic structure. The superconducting junction's critical current is sensitive to the stray magnetic fields generated by the ferromagnet, allowing us to indirectly monitor magnetization changes, see Fig. 1. Because the readout current is confined to the superconducting wire, no current

passes through the ferromagnet and no magnetization misalignment in the current path is required. This combination enables a readout scheme with minimal power dissipation, low susceptibility to bit corruption due to read-induced disturbances, realized with low device complexity.

As a proof of principle, we investigate CIMS in polycrystalline cobalt (Co) deposited directly on top of a superconducting aluminum (Al) wire. A training current is passed through the ferromagnet to induce a switching event that modifies the local stray-field distribution. The critical supercurrent I_c of the Al wire is sensitive to this change, as demonstrated in our previous experimental and simulation studies,^{15–17} enabling a readout that scales with the near-field stray-field amplitude.

The device consists of a superconducting Al wire and the ferromagnetic Co structure placed on top of the wire, forming a S–(S/F)–S junction, as shown in Fig. 2. A four-point configuration is used to measure the junction's current-voltage $V(I)$ and differential resistance $dV/dI(I)$ transport characteristics. The Co structure is separately contacted to allow application of a training current I_{train} through the ferromagnet to induce CIMS. All measurements are performed at 200 mK in a dilution refrigerator.

As the first step, the magnetization of the sample is initialized into a state of relatively low magnetization. A strong external magnetic field of 2T is applied along the $-y$ direction, parallel to the Co finger, followed by an opposing training field of -180 mT. This placed the

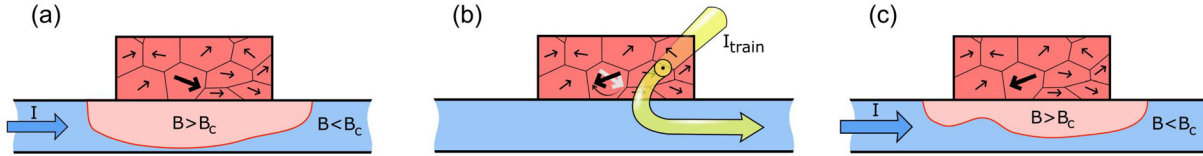


FIG. 1. Sketch of the CIMS detection via I_c . (a) Before the CIMS, the stray fields of the ferromagnet penetrate the superconducting wire below. Regions that experience fields $B > B_c$ become normal conducting, only regions with $B < B_c$ can still support supercurrent, limiting I_c . (b) Passing a current through the ferromagnet induces a CIMS. For visualization, we cartoon a situation in which the magnetization of a single grain (bold black arrow) is flipped by the CIMS. (c) After CIMS, the changed magnetization influences the stray-field distribution. Consequently, the distribution of normal conducting and superconducting regions changes, which impacts the critical current I_c of the junction.

ferromagnet in a remanent state of reduced magnetization when the external field is removed. This is visible by a finite I_c of the superconducting wire. In this low-magnetization state, the magnetic domains in the ferromagnet are misaligned chaotically and separated by domain walls.

In this magnetic configuration, training currents are applied to the ferromagnet in the form of slowly ramped pulses lasting several minutes, which minimizes thermal and electrical stress. After each training pulse, the system is allowed to thermally stabilize for ≈ 3 min before transport measurements are performed.

Step by step, the training-current amplitude is increased. After each pulse, with both the external field B and I_{train} set to zero, the transport properties and the critical current I_c of the superconducting junction are measured. Thereby, only persistent changes in the ferromagnet's magnetization are probed.

Figure 3 shows the critical current of the junction as a function of the previously applied I_{train} pulse. After $I_{\text{train}} = 450 \mu\text{A}$, corresponding to a current density of $J_{\text{CIMS}} \approx 1 \times 10^{10} \text{ A/m}^2$, a jump in I_c is observed. The transport characteristics before and after the jump are shown in Figs. 3(b) and 3(c) and 3(d) and 3(e), respectively. The $V(I)$ curves reveal the characteristic non-dissipative supercurrent at currents smaller than I_c , which jump from a relatively low I_c to a significantly higher I_c after the training with $450 \mu\text{A}$. The same change of I_c is observed in the differential resistance $dR(I) = dV(I)/dI$ as a shift of the peak position. The value for I_c in (a) is extracted from the peak position in the $dR(I)$ measurement.

In our previous studies,^{15–17} we could correlate these I_c jumps with abrupt changes in the magnetization of the ferromagnet, caused by individual domains that flip their orientation. Following these findings, we interpret the present observations as domain flips caused by CIMS, that in turn change the stray-field distribution around the ferromagnet and thereby the I_c of the S–(S/F)–S junction.

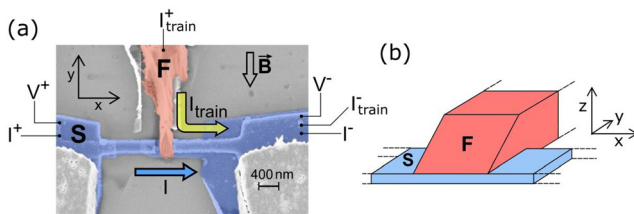


FIG. 2. (a) Colored SEM micrograph and (b) sketch of the three-dimensional geometry. The superconducting wire (blue) is placed below the ferromagnetic finger (red) directly on top of the substrate (not shown).

Significantly higher training currents, up to 10 mA, were applied to verify if electromigration is the cause of the observed changes. Even after such high current pulses, the junction relaxed to its original transport characteristics, demonstrating that the high currents cause no permanent modification of the structure. At 10.6 mA, the junction was eventually destroyed.

It is important to note that the $I_c(I_{\text{train}})$ -behavior is not in detail reproducible. In multiple training sequences, only a minority feature a CIMS event. The variations stem from the fact that the magnetization state, and therefore also the I_c value, after the initialization in magnetic field is not quantitatively reproducible. The magnetization behavior in the polycrystalline Co is chaotic and therefore the starting configuration for the CIMS measurements are not identical in repeated measurements.^{15–17} As possible STT contributions strongly depend on the local microscopic alignment of individual magnetic domains,¹⁸ a change in the magnetization configuration has a significant influence on the current needed to induce a CIMS. The same is true for the relative alignment of magnetic domains and Oersted fields. A weakly pinned domain in a region with high Oersted fields is switched by lower I_{train} than in a region of low Oersted fields.

The currents observed to show CIMS in this sample are on the order of $J_{\text{CIMS}} \approx 1 \times 10^{10} \text{ A/m}^2$. The uncertainty of this value is significant, as the ferromagnetic structure has a nontrivial geometry with nonuniform cross-sectional area A . For all current-density estimates, we assume a cross-sectional area $A = 176 \times 274 \text{ nm}^2$ (see the supplementary material for details). Moreover, since the training currents are always increased stepwise, the experimental procedure is inherently biased toward detecting low- J_{CIMS} events, while higher switching thresholds may remain outside the chosen measurement range.

In micromagnetic simulations performed with MuMax3,^{19–21} we can replicate the experimental observations and validate the discussed interpretation. In the first step, the magnetization switching is modeled using a basic Zhang–Li spin transfer torque model under consideration of Oersted fields in the micromagnetic framework.¹⁹ In a second step, the influence of the CIMS on the superconductor's I_c is modeled by a purely stray-field-dependent critical supercurrent model developed in Ref. 16.

The magnetic simulation considers the demagnetization field, exchange interaction, crystalline uniaxial anisotropy, external fields or Oersted fields and the Zhang–Li spin transfer torque τ_{STT} to model the magnetization behavior under applied fields or electric currents,

$$\tau_{\text{STT}} = \frac{1 + \zeta\alpha}{1 + \alpha^2} \mathbf{m} \times (\mathbf{m} \times (\mathbf{u} \cdot \nabla) \mathbf{m}) + \frac{\zeta - \alpha}{1 + \alpha^2} \mathbf{m} \times (\mathbf{u} \cdot \nabla) \mathbf{m},$$

where \mathbf{u} is a drift vector proportional to the current density \mathbf{J} : $\mathbf{u} = \frac{\mu_B P}{2e\gamma_0 M_{\text{sat}}(1 + \zeta^2)} \mathbf{J}$. The Zhang–Li STT does not require an externally

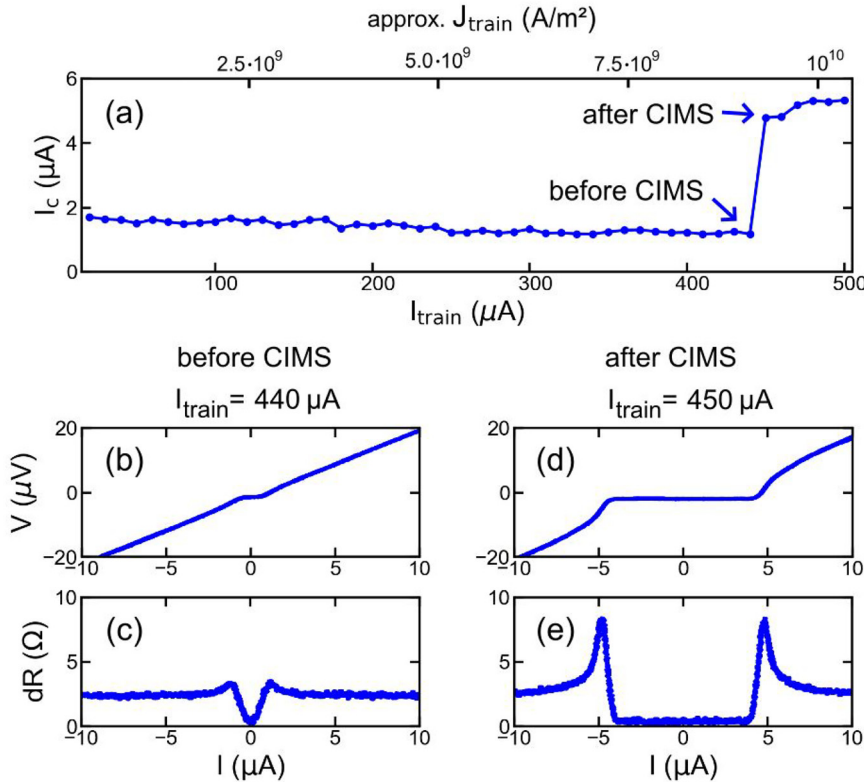


FIG. 3. Experimental $I_c(I_{\text{train}})$ data and $V(I)$ and $dR(I)$ curves before and after a CIMS. After application of $I_{\text{train}} = 450 \mu\text{A}$, a CIMS event changes the remanent magnetization configuration with a significant influence on the critical current I_c supported by the S-wire. For the underlying experimental data and details of the measurement, see modified from Kammermeier, "Magnetization-dependent critical current in S-(S/F)-S junctions: Experimental realization and micromagnetic simulation," Doctoral thesis (University of Konstanz, Konstanz, Germany, 2025). Copyright 2025 Authors, licensed under CC BY 4.0.¹⁷

polarized current; instead, it arises solely from the spatial gradient of the magnetization $\nabla \mathbf{m}$ at domain walls, relative to the current direction $\mathbf{J} \parallel \mathbf{u}$. This makes the model ideal for describing STT at three-dimensional domain walls in polycrystalline ferromagnets. Dzyaloshinskii–Moriya interaction (DMI), higher-order and nonlocal STT contributions, as well as SOT are neglected in this basic model. Also, temperature effects are negligible in this low-temperature setting (see the [supplementary material](#)). The material parameters used for Co are given in [Table I](#).

The simulated geometry is a polycrystalline Co structure closely following the experimental shape of the ferromagnet as sketched in [Fig. 2](#). The simulation uses a grain size of 40 nm and a cell size of $2 \times 2 \times 2 \text{ nm}^3$ within a $500 \times 486 \times 96 \text{ nm}^3$ simulation box. This atomic force microscopically determined value of the grain size has been found to adequately reproduce the experimental magnetic field

TABLE I. Material parameters used in the MuMax3 simulation.

Parameter	Value	Description
M_{sat}	$1.43 \times 10^6 \text{ A/m}$	Saturation magnetization ^{22–24}
A_{ex}	$2.6 \times 10^{11} \text{ J/m}$	Exchange stiffness ^{22,23}
α	0.02	Gilbert damping parameter
K_u	$6.8 \times 10^5 \text{ J/m}^3$	Uniaxial anisotropy constant ^{22–24}
ζ	0.01	Non-adiabaticity of STT ²⁵
P	0.42	Spin polarization of the current ²⁶

driven I_c changes observed in [Ref. 15](#). Each grain is assigned a random uniaxial anisotropy direction. A reduced grain–grain exchange coupling is modeled by attributing a 10% reduced exchange stiffness to cells at grain boundaries.

The simulation procedure follows the experimental procedure as closely as possible, see [Fig. 4](#).

- (1) Initialization in external field: Identical to the experiment, a strong external field of 2T is applied to saturate the magnetization. This is followed by an external field of -180 mT in the opposite direction to set an initial low-magnetization state. For the training in external field, the "minimize()" function evolves the magnetization iteratively into a local energy minimum via a steepest-descent method,²⁰ ideal for computing remanent states without involving time-dependent magnetization dynamics. The field is set to zero, and minimized again. This remanent magnetization state serves as the starting point for simulations with training currents.
- (2) Current training: The training current is applied in the $-y$ direction with current density J_{train} , along the long direction of the F-wire. The current density is modeled as constant throughout the ferromagnet and parallel to the $-y$ direction for simplicity. Whenever a training current is applied, also Oersted fields are applied in the simulation. The Oersted field B_{Oe} is modeled as radially symmetric $B_{\text{Oe}}(r) \propto r$, where r is the radius measured from the center of the F-wire (for details see the [supplementary material](#)). The consideration of Oersted fields significantly reduces the current densities needed to flip the

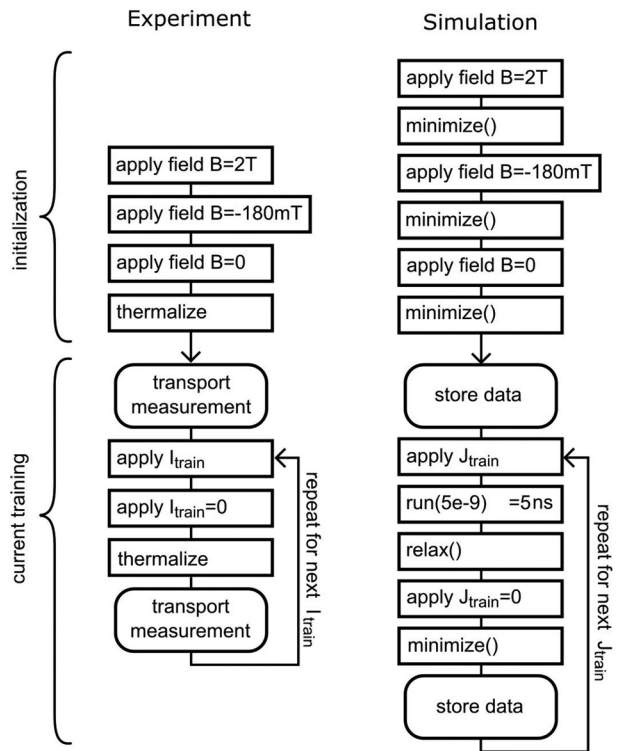


FIG. 4. Flow chart of the experimental and simulated current training sequence. First the initial magnetization configuration is set through application of external magnetic fields (initialization) and after that training currents are temporarily applied, to study the remanent magnetization change after the current is removed. These training currents are step by step increased in order to observe a CIMS event (current training).

magnetization compared to simulation runs that only consider STT, and is thereby a mandatory component of the simulation (see the [supplementary material](#)). The modeling of the STT requires the time-dependent approach of solving the Landau-Lifshitz-Gilbert (LLG) equation in time steps using the “run ()” method. A runtime of 5 ns proves to be sufficient to capture the full domain switching (see the [supplementary material](#)). This is followed by a “relax ()” operation to ensure a converged magnetization state. Thereafter, the training current is reduced to 0, followed by a steepest-descent energy minimization with `minimize ()`, to find the remanent magnetization state after the training. In this remanent state, the stray-field distribution as well as magnetization configuration is stored ([Fig. 5](#)).

The current application is then repeated step by step for increasing current densities from 0 to $1.1 \times 10^{10} \text{ A/m}^2$ in $0.1 \times 10^{10} \text{ A/m}^2$ steps. [Figure 6\(a\)](#) shows the normalized magnetization m of the ferromagnet as a function of the previously applied training current density J_{train} . It is important to note here that only remanent states are investigated, no training currents flow while the data are recorded.

Above a certain training current threshold, called J_{CIMS} , the magnetization amplitude m changes, because a single domain or a small

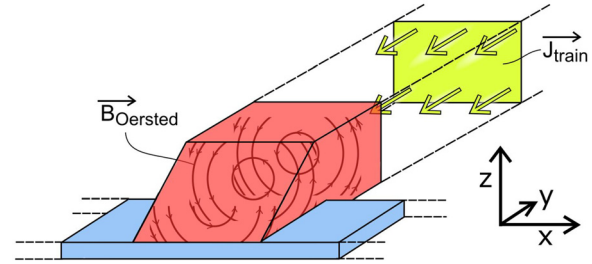


FIG. 5. Sketch of the spatially invariant applied training current density J_{train} and the Oersted field distribution B_{Oe} .

cluster flips its orientation due to the combined forces of STT and Oersted fields. m is normalized to a fully magnetized parallel alignment with $m = 1$. In the presented example $J_{\text{train}} = 0.7 \times 10^{10} \text{ A/m}^2 = J_{\text{CIMS}}$ triggers the CIMS. [Figure 6\(c\)](#) shows the magnetization distribution \mathbf{m} before and after the CIMS event in a cut through the ferromagnet. The position of the cut is sketched as green slice through the simulated structure for visualization.

This micromagnetic simulation provides, among many other aspects, the stray-field distribution around the ferromagnet [see [Figs. 6\(d\)](#) and [6\(e\)](#)] as a function of the preceding training current amplitude. Following the exact same method as in [Ref. 16](#), from this spatial stray-field distribution we can estimate a critical current of the S-wire below the F. The resulting simulated $I_c(J_{\text{train}})$ estimate is plotted in [Fig. 6\(b\)](#). The computation of I_c is based on the model that the local supercurrent density is dependent on the local stray-field amplitude, as shown in [Ref. 16](#). The white contours in [Figs. 6\(d\)](#) and [6\(e\)](#) correspond to the critical magnetic field of the superconductor. Before the CIMS, the field penetrated deeper into the S. The reduced stray fields after the CIMS increase the local critical supercurrent density supported in the S-wire, which in turn supports a higher critical current I_c .

These simulation results show that a CIMS within the experimental polycrystalline Co is a plausible explanation for the observed jump in I_c during current training. The experimental current densities are sufficient to switch magnetic domains when considering STT and B_{Oe} . This switching event changes the stray-field distribution around the F, and we show that the resulting change is large enough to affect the critical current of the S-wire by magnitudes similar to those observed in the experiment.

So far, we have only shown one selected simulated current-training sequence. However, the current density to induce a switching event, J_{CIMS} , is strongly dependent on the initial magnetic state, which itself is strongly dependent on the grain distribution within the F. Simulations were performed for many grain distributions resulting in J_{CIMS} values up to 10^{12} A/m^2 (see the [supplementary material](#)). The results in [Fig. 6](#) present a selected event that exhibits characteristics similar to those observed experimentally.

Also within one fixed grain distribution, variations in the initial state occur due to the chaotic nature of the initialization in external field,¹⁶ resulting in some training runs with J_{CIMS} similar to the experimental values, and some training runs with J_{CIMS} outside the experimental measurement range. Detailed information can be found in the [supplementary material](#).

The experiment shows fundamentally the same behavior. Only when the experimental initial state is suitable to feature a CIMS within

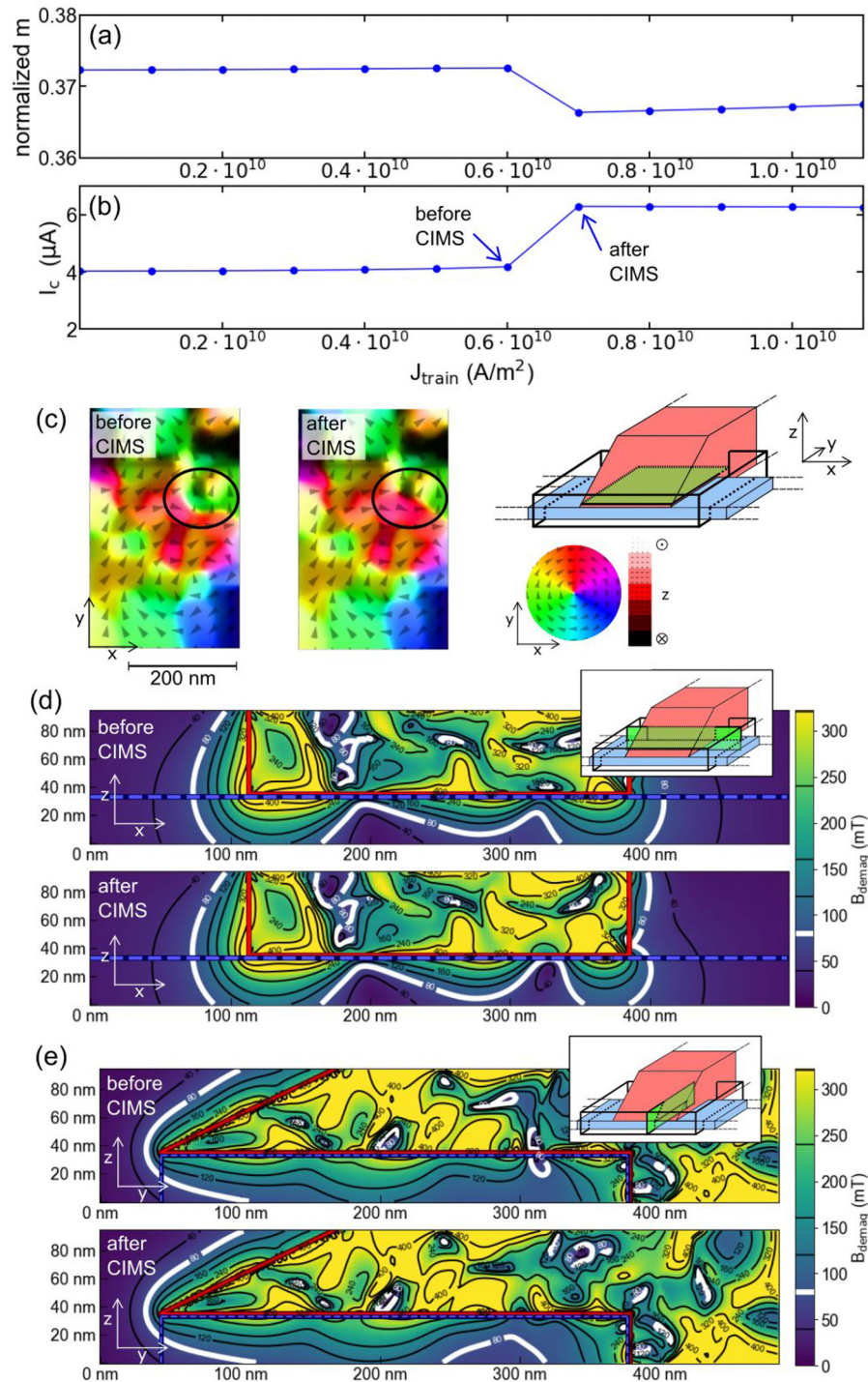


FIG. 6. (a) Simulated magnetization of the ferromagnet $m(J_{\text{train}})$ as a function of the training current density. (b) Resulting critical current $I_c(J_{\text{train}})$ of the superconducting wire, computed from the simulated stray-field distribution. The application of $0.7 \times 10^{10} \text{ A/m}^2$ causes a CIMS, that reduced m and increases I_c . (c) Color-coded vector representation of the local magnetic moments \mathbf{m} in a slice through the ferromagnet near the S-F interface, as sketched in green in the right scheme. One domain flips its orientation during the CIMS, indicated by a black circle. (d) and (e) The stray-field distribution B_{demag} around the ferromagnet (red box) and inside the superconductor (blue dashed box). Two cuts are shown before and after the CIMS. The white contour indicates the 80 mT line, as the critical magnetic field of the superconductor is $B_c = 80 \text{ mT}$. The field distribution changes locally during the CIMS. I_c is calculated from the stray-field distribution within the superconductor, following the methodology of Ref. 16.

the experimentally accessible current-density range, the switching is detected. Thereby, we can relate the low occurrence of detectable CIMS events in the experiment to the chaotic randomness of the initial magnetization state before the current training.

In summary, we have demonstrated that current-induced magnetization switching (CIMS) in a polycrystalline ferromagnet can be detected via the critical current of an adjacent superconducting wire. Stepwise current training induces abrupt domain flips in the ferromagnet, which modify the local stray-field distribution around it and thereby lead to a measurable jump in the superconducting wire's critical current.

Micromagnetic simulations based on the combined effects of Zhang-Li STT and Oersted fields reproduce these observations and connect the microscopic behavior within the ferromagnet to the macroscopically measured critical current of the superconductor. This CIMS detection approach provides a low-power readout method for magnetic switching devices, with potential applications in superconducting logics and low-temperature memory devices. The simplicity of the structure, combined with the fact that the readout current does not pass through the ferromagnet, makes it an attractive alternative for low-power magnetic readout.

Looking ahead, this readout scheme could be easily integrated into existing CIMS architectures to achieve repeatable and reversible switching. An ideal candidate would be a bi-layer binary switch with a parallel and an antiparallel magnetization state.^{13,27,28} When such a bi-layer structure is placed on top of a superconducting wire, the two magnetic configurations generate distinct stray-field patterns. These translate into measurable differences in the superconducting critical current, distinguishing between the high and low stray-field configuration.

See the [supplementary material](#) for a discussion of the experimental current density, demonstration showing that 5 ns is a sufficient runtime for the CIMS simulation, illustration of the temperature sensitivity of the simulation, and statistical variations arising from the simulated grain distribution and initial magnetization configuration. We also highlight the significance of the Oersted field contribution compared to pure STT runs and the influence of differing Oersted field models.

We acknowledge the use of experimental equipment and the expert support concerning its usage provided by the Nanostructure Laboratory at the University of Konstanz as well as access to local computing resources through the core facility Scientific Compute Cluster Konstanz (SCCKN). This work was financially supported by the Deutsche Forschungsgemeinschaft (DFG, German Research Foundation)—Project IDs 317077841 and 553541898.

AUTHOR DECLARATIONS

Conflict of Interest

The authors have no conflicts to disclose.

Author Contributions

Lukas Kammermeier: Conceptualization (lead); Data curation (lead); Formal analysis (lead); Visualization (lead); Writing – original draft (lead); Writing – review & editing (equal). **Elke Scheer:** Project administration (lead); Supervision (lead); Writing – review & editing (equal).

DATA AVAILABILITY

The data that support the findings of this study are available from the corresponding author upon reasonable request.

REFERENCES

- A. Hirohata, K. Yamada, Y. Nakatani, I.-L. Prejbeanu, B. Diény, P. Pirro, and B. Hillebrands, "Review on spintronics: Principles and device applications," *J. Magn. Magn. Mater.* **509**, 166711 (2020).
- B. Chen, M. Zeng, K. H. Khoo, D. Das, X. Fong, S. Fukami, S. Li, W. Zhao, S. S. Parkin, S. Piramanayagam, and S. T. Lim, "Spintronic devices for high-density memory and neuromorphic computing—A review," *Mater. Today* **70**, 193–217 (2023).
- M. Gajek, J. J. Nowak, J. Z. Sun, P. L. Trouilloud, E. J. O'Sullivan, D. W. Abraham, M. C. Gaidis, G. Hu, S. Brown, Y. Zhu, R. P. Robertazzi, W. J. Gallagher, and D. C. Worledge, "Spin torque switching of 20 nm magnetic tunnel junctions with perpendicular anisotropy," *Appl. Phys. Lett.* **100**, 132408 (2012).
- S. Bhatti, R. Sbiaa, A. Hirohata, H. Ohno, S. Fukami, and S. Piramanayagam, "Spintronics based random access memory: A review," *Mater. Today* **20**, 530–548 (2017).
- G. Yu, P. Upadhyaya, and Y. Fan, "Switching of perpendicular magnetization by spin-orbit torques in the absence of external magnetic fields," *Nat. Nanotechnol.* **9**, 548–554 (2014).
- B. Dai, M. Jackson, Y. Cheng, H. He, Q. Shu, H. Huang, L. Tai, and K. Wang, "Review of voltage-controlled magnetic anisotropy and magnetic insulator," *J. Magn. Magn. Mater.* **563**, 169924 (2022).
- L. Liu, C.-F. Pai, Y. Li, H. W. Tseng, D. C. Ralph, and R. A. Buhrman, "Spin-torque switching with the giant spin Hall effect of tantalum," *Science* **336**, 555–558 (2012).
- D. Kumar, T. Jin, R. Sbiaa, M. Kläui, S. Bedanta, S. Fukami, D. Ravelosona, S.-H. Yang, X. Liu, and S. Piramanayagam, "Domain wall memory: Physics, materials, and devices," *Phys. Rep.* **958**, 1–35 (2022).
- S. S. P. Parkin, M. Hayashi, and L. Thomas, "Magnetic domain-wall racetrack memory," *Science* **320**, 190–194 (2008).
- J.-L. Bello, Y. Quessab, J.-W. Xu, M. Vergès, H. Damas, S. Petit-Watlot, J.-C. R. Sánchez, M. Hehn, A. D. Kent, and S. Mangin, "Field-free current-induced magnetization switching in GdFeCo: A competition between spin-orbit torques and Oersted fields," *J. Appl. Phys.* **132**, 083903 (2022).
- S. V. Aradhya, G. E. Rowlands, J. Oh, D. C. Ralph, and R. A. Buhrman, "Nanosecond-timescale low energy switching of in-plane magnetic tunnel junctions through dynamic Oersted-field-assisted spin Hall effect," *Nano Lett.* **16**, 5987–5992 (2016).
- A. Manchon, J. Železný, I. M. Miron, T. Jungwirth, J. Sinova, A. Thiaville, K. Garello, and P. Gambardella, "Current-induced spin-orbit torques in ferromagnetic and antiferromagnetic systems," *Rev. Mod. Phys.* **91**, 035004 (2019).
- J. A. Katine, F. J. Albert, R. A. Buhrman, E. B. Myers, and D. C. Ralph, "Current-driven magnetization reversal and spin-wave excitations in Co/Cu/Co pillars," *Phys. Rev. Lett.* **84**, 3149 (2000).
- G. Sala, V. Krizakova, E. Grimaldi, C.-H. Lambert, T. Devolder, and P. Gambardella, "Real-time Hall-effect detection of current-induced magnetization dynamics in ferrimagnets," *Nat. Commun.* **12**, 656 (2021).
- L. Kammermeier and E. Scheer, "Magnetization control of the critical current in a S-(S/F)-S superconducting switch," *Appl. Phys. Lett.* **124**, 162605 (2024).
- L. Kammermeier and E. Scheer, "Micromagnetic simulation of the magnetization-controlled critical current in a S-(S/F)-S superconducting switch," *Appl. Phys. Lett.* **125**, 052602 (2024).
- L. Kammermeier, "Magnetization-dependent critical current in S-(S/F)-S junctions: Experimental realization and micromagnetic simulation," Doctoral thesis (University of Konstanz, Konstanz, Germany, 2025).
- T. Horaguchi, M. Matsuo, and Y. Nozaki, "Highly accurate evaluation of spin-torque efficiency by measuring in-plane angular dependence of spin-torque ferromagnetic resonance," *J. Magn. Magn. Mater.* **505**, 166727 (2020).
- A. Vansteenkiste, J. Leliaert, M. Dvornik, M. Helsen, F. Garcia-Sanchez, and B. V. Waeyenberge, "The design and verification of MuMax3," *AIP Adv.* **4**, 107133 (2014).

- ²⁰L. Exl, S. Bance, F. Reichel, T. Schrefl, H. P. Stimming, and N. J. Mauser, "Labonte's method revisited: An effective steepest descent method for micromagnetic energy minimization," *J. Appl. Phys.* **115**, 17D118 (2014).
- ²¹J. Leliaert, B. V. de Wiele, A. Vansteenkiste, L. Laurson, G. Durin, L. Dupré, and B. V. Waeyenberge, "Current-driven domain wall mobility in polycrystalline permalloy nanowires: A numerical study," *J. Appl. Phys.* **115**, 233903 (2014).
- ²²S. Egle, C. Bacca, H. Pernau, M. Huefner, D. Hinzke, U. Nowak, and E. Scheer, "Magnetoresistance of atomic-size contacts realized with mechanically controllable break junctions," *Phys. Rev. B* **81**, 134402 (2010).
- ²³C. Wen-Bing, H. Man-Gui, Z. Hao, O. Yu, and D. Long-Jiang, "Micromagnetic simulation on the dynamic susceptibility spectra of cobalt nanowires arrays: The effect of magnetostatic interaction," *Chin. Phys. B* **19**(8), 087502 (2010).
- ²⁴L. D. Buda, I. L. Prejbeanu, U. Ebels, and K. Ounadjela, "Micromagnetic simulations of magnetisation in circular cobalt dots," *Comput. Mater. Sci.* **24**, 181–185 (2002).
- ²⁵S. Zhang and Z. Li, "Roles of nonequilibrium conduction electrons on the magnetization dynamics of ferromagnets," *Phys. Rev. Lett.* **93**, 127204 (2004).
- ²⁶E. Y. Tsybal and I. Zutic, *Handbook of Spin Transport and Magnetism* (Chapman and Hall/CRC, New York, 2012).
- ²⁷F. J. Albert, N. C. Emley, E. B. Myers, D. C. Ralph, and R. A. Buhrman, "Quantitative study of magnetization reversal by spin-polarized current in magnetic multilayer nanopillars," *Phys. Rev. Lett.* **89**, 226802 (2002).
- ²⁸D. Ralph and M. Stiles, "Spin transfer torques," *J. Magn. Magn. Mater.* **320**(7), 1190–1216 (2008).